Orbits of swimmers around obstacles

Dario Papavassiliou[1,*] and Gareth P. Alexander[1]

[1]*Department of Physics and Centre for Complexity Science, University of Warwick, Coventry, CV4 7AL, UK*

We present a two dimensional model of hydrodynamic interaction between a circular swimmer and a circular post at low Reynolds number, using a point singularity description of the swimming activity. We derive a nonlinear dynamical system fully describing the motion and discuss the generic features of the phase portrait and typical trajectories for a variety of squirmer modes. Contractile swimmers exhibit stable bound orbits arising from the contrasting nature of monopolar and dipolar squirmer modes, which are robust with respect to swimmer size and the inclusion of higher squirmer modes. The behaviour of extensile swimmers is related through time reversal and their orbits are unstable, in qualitative agreement with experimental observations.

I. INTRODUCTION

Active microscopic swimmers, such as bacteria [1] or self-propelled particles [2–4], are known to exhibit behaviour which can only be explained by considering the role of the suspending fluid [5, 6]. Hydrodynamic interactions with surfaces result in observed circling and scattering behaviour of bacteria [7–11] and following of boundaries by both artificial and natural swimmers [12, 13]. Interactions between active particles are responsible for the 'waltzing' of *Volvox* colonies [14] and synchronisation of flagellar beating [15], and, at high densities of contractile active particles, the generic instability of the isotropic phase [16–18]. Otherwise immobile active particles, which only stir the fluid medium, can be set in motion by obstacles in the fluid [14, 19, 20]. Much experimental work is currently taking place seeking to exploit such effects for micro-technological applications, for example directing efficient microscopic mass transport [21, 22], or extracting work from a bacterial bath to drive devices [23].

Recent experiments have measured the flow field produced by swimming microorganisms, for example the algae *Chlamydomonas* and *Volvox* [24] and the bacterium *Escherichia coli* [9], finding a complex flow field that depends strongly on the microscopic details near the swimmer and has the dipolar structure characteristic of force-free motion at larger distances [18, 25]. Hydrodynamic interactions are often modelled purely in terms of this dipolar flow [6, 16, 26], reproducing the tendency for individual swimmers to follow walls [20] and the generic hydrodynamic behaviour of suspensions [16–18]. This asymptotic flow characterises swimmers as *extensile* or *contractile* according to the sign of the dipole [18]. However, the head-tail symmetry of the flow does not capture the swimming direction. As such active particles that faithfully mimic dipolar flows are *apolar* and immotile, although their activity circulates the fluid and drives motion close to boundaries [14] or through inter-particle interactions [27, 28]. For a particle to swim there must necessarily be additional, non-dipolar contributions to the flow field. The tangential slip velocity induced by the swimmer on its surface may be decomposed into discrete Fourier modes, or *squirmer modes* [29, 30]. Then the swimmer speed is set by the amplitude of the first squirmer mode, so that a minimal description for swimmers is a superposition of this mode and the second squirmer mode, which gives precisely the dipolar flow field generated by a force dipole.

Using this minimal model, we study the hydrodynamic interactions of a swimmer with a fixed circular post in two dimensions and characterise its behaviour in terms a dynamical system governing the swimming trajectories. This extends previous work on the effects of swimming close to a wall [20] to the case of finite-sized boundaries. We find a wide range of behaviours including trapping in bound states around a stable circular orbit and scattering, that are robust to the inclusion of higher-order squirmer modes in the slip velocity and the relative size of the swimmer and post. The behaviour of contractile and extensile swimmers is found to be related by time reversal [31], resulting in instability of the generic orbits of extensile swimmers. These results are relevant to several recent experiments on active matter that are quasi-two-dimensional, involving sedimented [13] or floating swimmers [19, 20], or samples confined to a thin layer [4]. Our results can also be expected to give a good qualitative flavour of behaviour in three dimensions as has been found in previous studies of two-dimensional fluid dynamics [20, 32–37].

*d.papavassiliou@warwick.ac.uk

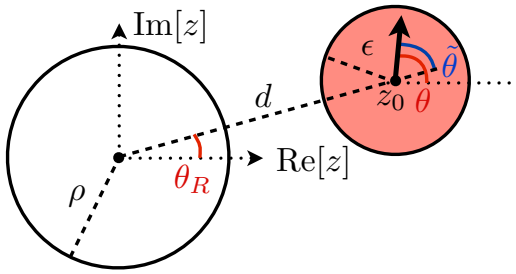

FIG. 1: A circular swimmer (pink) of radius ϵ centred at the point $z_0 = de^{i\theta_R}$ exterior to a post of radius ρ at the origin. The swimmer's head makes an angle θ with the real axis and $\tilde{\theta}$ (blue) with the radial direction joining the two centres.

II. COMPLEX FORMULATION OF HYDRODYNAMICS

At the microscopic length scales relevant to natural and artificial examples of active matter, the medium behaves as an incompressible viscous fluid and the flow field $\boldsymbol{u}$ is described by the Stokes equations, $-\boldsymbol{\nabla} p + \eta \nabla^2 \boldsymbol{u} = \boldsymbol{0}$ and $\boldsymbol{\nabla} \cdot \boldsymbol{u} = 0$, where p is the pressure and η the viscosity. A two-dimensional Stokes flow $\boldsymbol{u} = (u, v)$ is conveniently expressed in terms of the streamfunction $\psi(x, y)$ satisfying the biharmonic equation, $\nabla^4 \psi = 0$. The solution can be written in terms of functions of the complex coordinate $z = x + \mathrm{i}y$ as $\psi(z, \overline{z}) = \mathrm{Im}[\overline{z} f(z) + g(z)]$. These *Goursat functions*, f and g, are analytic in the fluid domain, except for isolated singularities, and are determined by the boundary conditions. Once these are found the flow is fully determined, since

$$\frac{p}{\eta} - \mathrm{i}\omega = 4f'(z), \qquad u + \mathrm{i}v = -f(z) + z\overline{f'(z)} + \overline{g'(z)} \tag{1}$$

where ω is the vorticity and primes denote a derivative taken with respect to the argument [38].

Stokes flows can be expressed using distributions of *Stokes singularities* [39] corresponding to point forces, torques, stresses and so on, which manifest themselves as singularities of the Goursat functions. We employ a variant of the *squirmer* model [26, 29, 30] defined in terms of such singularities. The swimmer is a disc of radius ϵ, with its centre located at the point $z_0 = de^{i\theta_R}$ and the direction of its head defined by the angle θ, as shown in figure 1. Traditionally the swimming action is determined by specifying the tangential flow on the surface, u_s, with its orientation determined by the swimmer's head. Instead we specify a set of Stokes singularities at z_0, reproducing the desired slip velocity in an unbounded domain. The presence of a non-slip boundary is then accounted for by image singularities chosen to cancel the flow on the boundary. These singularities modify the flow near the swimmer, altering its translational and rotational motion and leading to a closed dynamical system describing its trajectories.

III. A DIPOLAR SQUIRMER

Self-propelled particles generically generate flows that are dipolar at large distances, so such a singularity should be included in any hydrodynamic description. At the point on the surface parametrised by the angle ϕ, a dipolar slip velocity is given by

$$u_s = 2V_2 \sin[2(\phi - \theta)], \tag{2}$$

while the flow normal to the surface is zero. The parameter V_2 has units of speed and quantifies the strength of the activity, but its choice is inconsequential to the dynamics because the Stokes equations are time-independent. It can be shown [20] that the Goursat functions $\tilde{f}(z)$, $\tilde{g}'(z)$ giving this surface flow can be expressed in terms of elementary singularities at z_0 as

$$\tilde{f}(z) = \frac{\epsilon V_2 e^{2i\theta}}{z - z_0}, \qquad \tilde{g}'(z) = \frac{2\epsilon^3 V_2 e^{2i\theta}}{(z - z_0)^3} + \frac{\overline{z_0}\epsilon V_2 e^{2i\theta}}{(z - z_0)^2}. \tag{3}$$

Note that such a swimmer will not move in an unbounded fluid, because the activity is head-tail symmetric.

In the presence of boundaries, the singularities (3) are reflected and give rise to images outside the fluid region. We consider the swimmer to be external to a stationary non-slip post, represented by a disc of radius ρ at the origin (see

figure 1). Then the condition of zero flow on the post surface is

$$u + \mathrm{i}v = -f(z) + z\overline{f'(z)} + \overline{g'(z)} = 0 \qquad \text{on} \qquad \overline{z} = \frac{\rho^2}{z}, \tag{4}$$

implying the functional relationship

$$g'(z) = \overline{f}\left(\frac{\rho^2}{z}\right) - \frac{\rho^2}{z} f'(z), \tag{5}$$

where $\overline{f}(z) \equiv \overline{f(\overline{z})}$, by which $g'(z)$ may be determined given a choice of $f(z)$. The minimal image singularity distribution consistent with (3) is

$$f(z) = \frac{\epsilon V_2 \mathrm{e}^{2\mathrm{i}\theta}}{z - z_0} + \frac{\delta}{z - \frac{\rho^2}{\overline{z_0}}} + \frac{\lambda}{\left(z - \frac{\rho^2}{\overline{z_0}}\right)^2} + \frac{\chi}{\left(z - \frac{\rho^2}{\overline{z_0}}\right)^3}, \tag{6}$$

for some complex coefficients δ, λ, χ, to be determined. A corresponding $g'(z)$ is given by (5), and matching its singularities at z_0 to those in (3) determines the unknown coefficients in terms of V, ϵ, z_0 and θ [20].

To determine the flow on the surface of the swimmer, we expand f and g' in the vicinity of $z = z_0$,

$$f(z) = \frac{\epsilon V_2 \mathrm{e}^{2\mathrm{i}\theta}}{z - z_0} + f_0 + f_1(z - z_0) + \dots \tag{7}$$

$$g'(z) = \frac{2\epsilon^3 V_2 \mathrm{e}^{2\mathrm{i}\theta}}{(z - z_0)^3} + \frac{\overline{z_0}\epsilon V_2 \mathrm{e}^{2\mathrm{i}\theta}}{(z - z_0)^2} + g_0 + \dots \tag{8}$$

where f_0, f_1, g_0 depend on δ, λ, χ (and can therefore be written in terms of V, ϵ, z_0 and θ). On the surface of the swimmer, the flow is due to activity plus motion, so that

$$u + \mathrm{i}v = \dot{z_0} + \epsilon\dot{\theta}\hat{t} + u_s\hat{t} \tag{9}$$

where a dot denotes a time derivative. For our disc the unit tangent $\hat{t}$ is given by $\mathrm{i}(z - z_0)/\epsilon$, and calculating the flow using (7) and (8) we obtain a dynamical system for d, θ and θ_R,

$$\dot{z_0} = \mathrm{e}^{\mathrm{i}\theta_R}(\dot{d} + \mathrm{i}d\dot{\theta}_R) = -f_0 + \overline{f_1} z_0 + \overline{g_0}, \qquad\qquad \dot{\theta} = -2\mathrm{Im}[f_1]. \tag{10}$$

Note that by rotational symmetry about the post, we expect that the motion should depend only on the difference in orientation between the swimmer's head and its alignment with the post,

$$\tilde{\theta} = \theta - \theta_R. \tag{11}$$

We indeed find this to be the case and henceforth retain this notation. The explicit dynamical system is

$$\dot{d} = -\frac{2V_2\epsilon d\cos 2\tilde{\theta}}{d^2 - \rho^2}\left(1 - \frac{\epsilon^2}{(d^2 - \rho^2)} - \frac{4\epsilon^2\rho^2}{(d^2 - \rho^2)^2}\right) \tag{12}$$

$$\dot{\theta} = 2V_2\epsilon\sin 2\tilde{\theta}\left(\frac{1}{d^2} - \frac{1}{d^2 - \rho^2} - \frac{\rho^2}{(d^2 - \rho^2)^2} + \frac{6\epsilon^2\rho^2}{(d^2 - \rho^2)^3} + \frac{6\epsilon^2\rho^4}{(d^2 - \rho^2)^4}\right) \tag{13}$$

$$\dot{\theta_R} = 2V_2\epsilon\sin 2\tilde{\theta}\left(\frac{1}{d^2} - \frac{1}{d^2 - \rho^2} - \frac{\rho^2}{d^4} - \frac{\epsilon^2}{(d^2 - \rho^2)^2} + \frac{2\epsilon^2\rho^2}{(d^2 - \rho^2)^3}\right). \tag{14}$$

Wall limit

When the post is infinitely large ($\rho \to \infty$) it becomes a planar wall, as considered previously by [20]. This limit is obtained by a linear transformation of the coordinate d to instead measure the distance y from the surface of the post to the swimmer, $y = d - \rho$. Upon fixing the orientation of the system with $\theta_R = \pi/2$ and transforming to Cartesian coordinates, we recover the dynamical system of a dipolar swimmer close to such a wall,

$$\begin{gathered}\dot{y} = \frac{V_2\epsilon\cos 2\theta}{y}\left(1 - \frac{\epsilon^2}{y^2}\right), \qquad \dot{\theta} = \frac{V_2\epsilon\sin 2\theta}{2y^2}\left(1 - \frac{3\epsilon^2}{2y^2}\right), \\ -(y + \rho)\dot{\theta}_R = \dot{x} = -\frac{V_2\epsilon\sin 2\theta}{y}\left(1 - \frac{\epsilon^2}{2y^2}\right).\end{gathered} \tag{15}$$

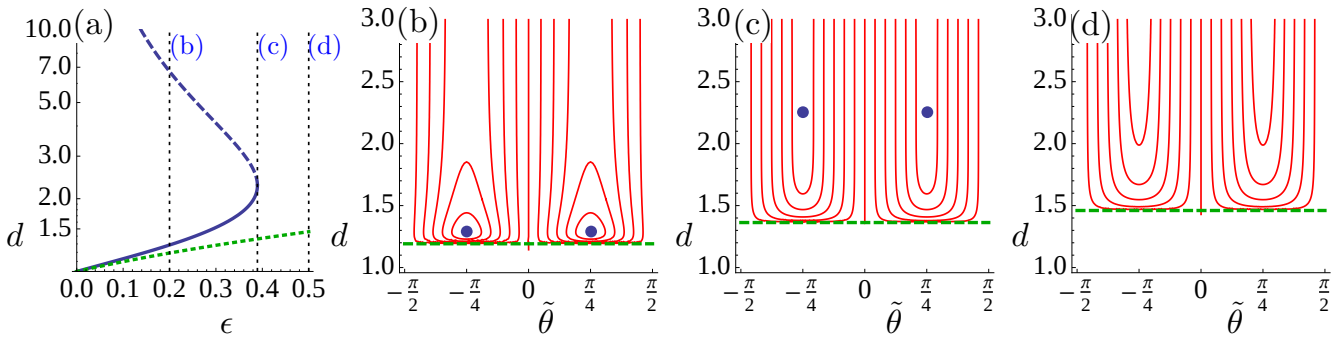

FIG. 2: Phase behaviour of dipolar swimmer close to a post as a function of swimmer size ϵ. **(a)** Existence of circular orbits (blue) compared to excluded radius (dashed green). The upper branch (dashed) of this bifurcation diagram is unstable. Orbits only exist for $\epsilon < \epsilon_c$ where $\epsilon_c \approx 0.38942$, at which point the single unstable orbit is at $d = d_o^* \approx 2.2681$. Trajectories in phase space are shown for **(b)** $\epsilon = 0.2$, **(c)** $\epsilon = \epsilon_c$, and **(d)** $\epsilon = 0.5$ with the blue dot marking the stable orbit and the dashed green line the excluded radius. For small values of ϵ there exist circular orbits with nearby non-circular periodic orbits. Increasing ϵ past the critical value ϵ_c the orbits close at infinity and the dynamical equations (16), (17) have no fixed point at distances greater than the excluded radius.

Then, $\dot{y}$ and $\dot{x}$ give the perpendicular and parallel components of the motion, respectively, and $\dot{\theta}$ the rotation. Analogous to the rotational symmetry of a finite-sized post, there is translational symmetry along the wall and the dynamical equations are independent of x.

Trajectories and phase behaviour

Returning to a finite-sized post, its radius ρ provides a natural unit of length for the system so we implicitly rescale all lengths accordingly. Similarly, we choose $\rho^2/V_2\epsilon$ as the unit of time, so that the combination $V_2\epsilon$ seen in equations (12)-(14) is equal to one unit of inverse time after lengths are rescaled to ρ. Exploiting rotational symmetry about the post it is convenient to combine (13) and (14) to give the reduced system

$$\dot{d} = \frac{2d\cos 2\tilde{\theta}}{d^2-1}\left(-1 + \frac{\epsilon^2}{(d^2-1)} + \frac{4\epsilon^2}{(d^2-1)^2}\right) \tag{16}$$

$$\dot{\tilde{\theta}} = 2\sin 2\tilde{\theta}\left(\frac{1}{d^4} + \frac{\epsilon^2-1}{(d^2-1)^2} + \frac{4\epsilon^2}{(d^2-1)^3} + \frac{6\epsilon^2}{(d^2-1)^4}\right). \tag{17}$$

The ratio of these equations,

$$\frac{\mathrm{d}d}{\mathrm{d}\tilde{\theta}} = -\frac{d^5(d^2-1)\big(d^4 - d^2(\epsilon^2+2) + (1-3\epsilon^2)\big)}{\epsilon^2 d^8 - 2(1-\epsilon^2)d^6 + (3\epsilon^2+5)d^4 - 4d^2 + 1}\cot 2\tilde{\theta}, \tag{18}$$

is separable and may be solved analytically to find an implicit equation for trajectories in the phase space of this reduced dynamical system.

At $\tilde{\theta} = \pm\pi/4$ we see fixed points for certain values of ϵ. These occur when the denominator of (18) is zero, and the bifurcation analysis in figure 2(a) reveals that these exist only for $\epsilon < \epsilon_c \approx 0.4$. From linear stability both branches are determined as centres, although numerical integration of the equations of motion suggests that the upper branch is unstable to small perturbations. Figures 2(a)-(c) show the phase portraits of the reduced dynamical system for three values of ϵ, below, at and above ϵ_c. The location of the stable centre is shown by a blue point.

The swimmer trajectories in real space are found by numerical integration of the equations of motion (12)-(14). These trajectories are driven solely by hydrodynamic interactions since purely dipolar squirmers are immotile. At the centre in phase space, the swimmer orbits the post at a fixed radius with its orientation relative to the post a constant $\pi/4$ (figure 3(a)). Close to this centre, orbits are eccentric, with periodic incursions towards the post. Both rotational and translational speed are highest at these incursions (figure 3(b)). The locations of these trajectories in phase space are shown in figure 3(c). For a swimmer size below ϵ_c all initial conditions are bound in such orbits, with the exception of the special cases $\tilde{\theta} = 0, \pm\pi/2$ where motion is purely linear. At and above the critical swimmer size all orbits close at infinity (figures 2(c)-(d)), so the post cannot trap the swimmer and we instead see deflections of the swimmer by the post.

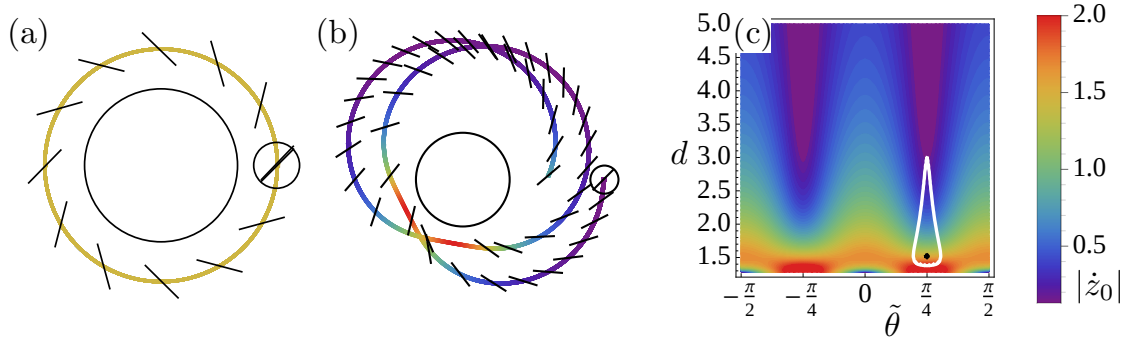

FIG. 3: Bound trajectories of a dipolar swimmer of radius $\epsilon = 0.3$ showing orientation and speed variation along path. **(a)** A circular orbit at $d_o \approx 1.52$. The orientation of the swimmer's head relative to the post is a constant $\pi/4$. **(b)** An eccentric orbit. Both translational and rotational speeds are highest at the portions of the orbit closest to the post. **(c)** Heat map of the dependence of translational speed $|\dot{z}_0|$ on distance and orientation relative to the post. The locations of the trajectories in phase space are shown in **(a)** black and **(b)** white.

A significant feature of these phase portraits is the emergence of a repulsion between the swimmer and the post. Equation (16) is solved independently of $\tilde{\theta}$ by two values of d^2 corresponding to radii through which trajectories cannot pass. Trajectories in the fluid region are bounded by the larger of these, d_r, which is given by

$$d_r = \sqrt{\frac{2 + \epsilon^2 + \epsilon\sqrt{16 + \epsilon^2}}{2}} = 1 + \epsilon - \frac{\epsilon^2}{4} + \dots \tag{19}$$

This excluded radius is shown as a dashed green line in figure 2. Remarkably this corresponds to hard repulsion between the post and the swimmer to linear order in ϵ despite the expected breakdown of this model at small separations, suggesting that the correct qualitative behaviour is captured by this model.

IV. GENERAL ACTIVITY PROFILES

Motile particles necessarily have non-dipolar contributions to their activity. In general, a physical surface flow is described by an infinite sum of squirmer modes

$$u_s = \sum_{n=1}^{\infty} u_{s_n}, \qquad \text{where} \quad u_{s_n} = 2V_n \sin[n(\phi - \theta)], \tag{20}$$

and is specified by the vector of mode amplitudes $(V_1, V_2, V_3, \dots)$. However, the singularity solutions corresponding to the n^{th} mode u_{s_n} contribute a flow field which decays as $(z - z_0)^{-n}$, so a good approximation to an arbitrary swimming profile can be made by considering only the first few of these modes, and indeed the minimal model of an active swimmer is the superposition

$$u_s = u_{s_1} + u_{s_2} = 2V_1 \sin[\phi - \theta] + 2V_2 \sin[2(\phi - \theta)], \tag{21}$$

in which the first term, the *monopole*, specifies the swimming speed V_1 (zero for apolar active matter) and the second term gives the correct far-field flow for a force dipole [29]. Then the classification of the swimming strategy is by a single real number, V_2/V_1, which is positive for a contractile swimmer and negative for an extensile swimmer. Note that for an apolar disc, *i.e.* with $V_1 = 0$, there is no distinction between contractile and extensile activity in two dimensions since they are identical under rotation by $\pi/2$.

Following analogous steps to those shown in § III, we are able to derive the equations of motion corresponding to each mode individually. Then, the equations of motion for a swimmer with a superposition of modes are simply a linear combination of those arising from the constituent pure modes.

The monopolar squirmer

The surface flow (21) differs from the pure dipole flow considered in § III by a monopolar squirming mode associated with the swimming speed V_1. While a swimmer with a purely monopolar flow field does not exhibit the far-field

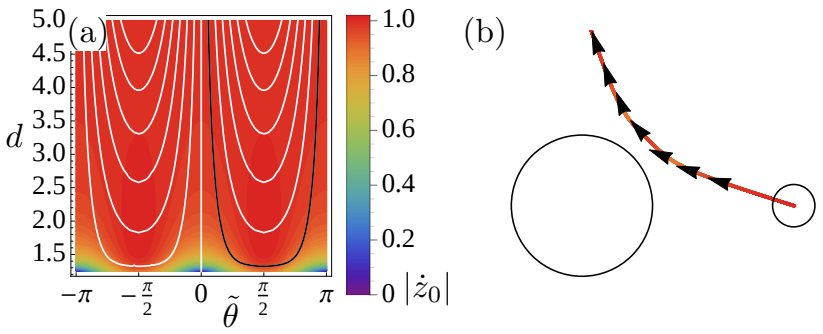

FIG. 4: Behaviour of a monopolar squirmer of size $\epsilon = 0.3$ near a circular post. **(a)** Speed $|\dot{z}_0|$ (colour) and trajectories (white) in phase space. There exist no bound orbits for any swimmer size. The black trajectory is shown in **(b)** together with arrows demonstrating orientation of the swimmer's head. Note that, unlike the dipolar swimmer, here there is a *decrease* in speed as the separation between the swimmer and the post decreases.

behaviour required of an active matter model, it is nevertheless instructive to study its behaviour before considering a superposition, since it is precisely the limit $V_2/V_1 \to 0$. The equations of motion corresponding to monopolar activity are

$$\dot{d} = V_1\left(1 - \frac{\epsilon^2}{(d^2-1)} - \frac{3\epsilon^2}{(d^2-1)^2}\right)\cos\tilde{\theta}, \qquad \dot{\theta} = -\frac{4V_1\epsilon^2 d}{(d^2-1)^3}\sin\tilde{\theta},$$
$$\dot{\theta}_R = \frac{V_1}{d}\left(1 + \frac{\epsilon^2}{(d^2-1)} - \frac{\epsilon^2}{(d^2-1)^2}\right)\sin\tilde{\theta}, \tag{22}$$

where once again lengths have been rescaled in units of the post radius ρ. As expected, equations (22) contain contributions that are independent of interactions with the post corresponding to self-propulsion. In contrast the dipolar swimmer, we do not find any bound trajectories. The hydrodynamic interaction with the post causes a deflection (figure 4), indicating that the self-propulsion is sufficient to cancel any attractive effect of the post. Furthermore, the interaction with the post serves to decrease, rather than increase, the swimming speed at small separations. As before, we see the emergence of an excluded volume interaction, with all trajectories in the fluid not coming closer than

$$d_r = 1 + \frac{\sqrt{3}}{2}\epsilon - \frac{\epsilon^2}{8} + \ldots \tag{23}$$

The effect of the deceleration close to the post can be seen by setting $\tilde{\theta} = \pi$ in equations (22). This one-dimensional system describing the time-evolution of d corresponds to a head-on collision of the swimmer with the post, and the time taken to collision, t_c, from an initial separation d_0 is given by

$$t_c = -\frac{1}{V_1}\int_{d_0}^{d_r}\left(1 - \frac{\epsilon^2}{(d^2-1)} - \frac{3\epsilon^2}{(d^2-1)^2}\right)^{-1}\mathrm{d}d. \tag{24}$$

This integral is logarithmically divergent for all values of d_0 and the swimmer size ϵ, so the hydrodynamic interaction causes collisions to require infinite time. (In practice, rotational diffusion of the swimmer, here ignored, would cause reorientation and deflection.)

Superposition of modes

The behaviour in the case of general activity depends on the interplay between squirmer modes but the key features are already apparent in the minimal model (21). The structure of the dynamics is a superposition of (12)-(14) and (22), reflecting the underlying linearity of the Stokes equations. From this the existence of fixed points in the phase portrait can be inferred. For instance, the phase flow along the line $\tilde{\theta} = 0$ is outwards from the monopolar mode and inwards from the dipolar mode (assuming V_1, V_2 both positive). Since these have different rates of decay they will be in balance at some distance corresponding to a saddle-point in the phase portrait. This saddle-point separates regions

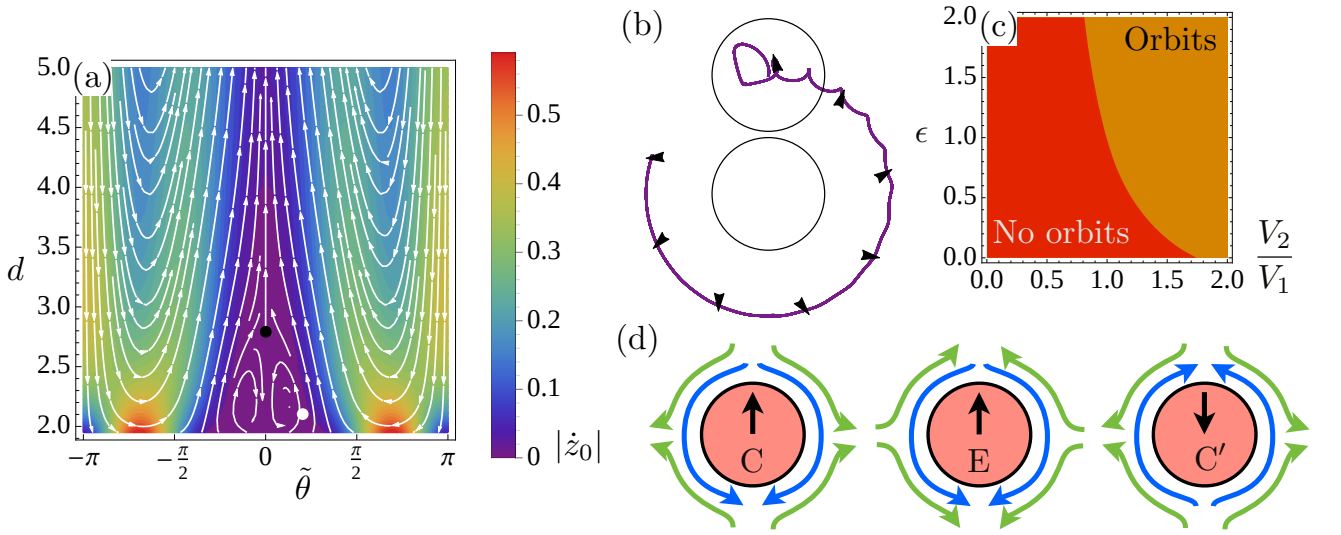

FIG. 5: **(a)** Phase portrait for a contractile swimmer of size $\epsilon = 1$ with $V_2/V_1 = 5/4$. Colour is speed. Features from the phase portraits of both individual modes are shown, such as closed cycles in the centre, and deflections for $|\tilde{\theta}| > \pi/2$. To obtain the phase portrait for the analogous extensile swimmer, reverse the direction of the arrows and shift the origin to $\tilde{\theta} = \pi$. **(b)** The trajectory given by the initial condition shown as a white point on **(a)**, showing evolution towards a circular orbit. **(c)** Existence of the saddle-point, in black on **(a)**, determining the existence of closed orbits, as a function of ϵ and V_2/V_1. In the red region this saddle point does not exist, while in the yellow region it does and we see orbits. This is consistent with the limits $V_2/V_1 \to 0$ and $V_2/V_1 \to \infty$, the monopolar and dipolar cases respectively. **(d)** Symmetry relating contractile (C) and extensile (E) swimmers. The monopolar and dipolar squirmer modes are shown schematically as blue and green arrows, respectively, and the black arrow gives the swimming direction. An extensile swimmer is mapped to a contractile swimmer by reversing time and exchanging the head and tail (C′).

of scattering off the post from the basin of attraction of a pair of spirals and guarantees bound orbits as a generic feature of the hydrodynamic interactions.

Figure 5(a) shows the phase portrait for a swimmer of equal size to the post ($\epsilon = 1$), with $V_2/V_1 = 5/4$ (therefore contractile), and figure 5(b) shows a typical bound orbit trajectory. Along the line $\tilde{\theta} = 0$ the phase flow reduces to the one-dimensional dynamical system $\dot{d} = h(d)$ for some rational function $h(d)$, and the saddle-point is located at a zero of $h(d)$. The parameter values for which this saddle-point exists within the fluid domain are shown in figure 5(c). The boundary between the regions of parameter space is given by the change in sign of the discriminant of the numerator of $h(d)$. Strikingly, these orbits exist for all swimmer sizes (provided the ratio of activities V_2/V_1 is sufficiently large) even though they were absent for monopolar activity and existed only in a restricted range for pure dipolar activity. Experiments on autophoretic rods also show orbits around spheres whose existence is not dependent on the size of the rod [13].

The phase portrait for extensile swimmers also exhibits the same generic structural features. Reversing the sign of the dipolar squirmer mode shifts the phase portrait by π along the $\tilde{\theta}$-axis and reverses the direction of the phase flow (figure 5(d)). Indeed, contractile and extensile swimmers can be mapped onto each other by a combination of time reversal and head-tail exchange, an example of the general symmetries of low Reynolds number swimming discussed by [31]. Therefore, we find a saddle-point in subject to exactly the same existence criteria as shown in figure 5(c), only now it demarcates a region of unstable spiral orbits. Whereas contractile swimmers are repelled from the surface, extensile swimmers are attracted and trajectories in this region typically lead to collision with the post. This general behaviour has been observed in *Chlamydomonas* [10].

Higher order squirmer modes do not appear to change these qualitative features as might be expected given their more rapid decay with distance.

V. DISCUSSION

We have analysed the hydrodynamic interactions between swimmers and finite-sized obstacles in two dimensions, extending previous work for swimmer interactions with a planar wall [20]. Stable bound orbits are shown to be

generic for contractile swimmers and robust with respect to swimming strategy and swimmer size, in broad qualitative agreement with recent experiments [10, 13]. Although the simple model we present is only accurate at large separations and breaks down in the near-field, an excluded volume interaction correct to linear order in the swimmer size emerges naturally. This suggests that the qualitative features it captures are reliable and it may help to explain the origin of different behaviour.

The circular post we have analysed here may be considered to be an idealisation of a general finite-sized object, around which a swimmer may be expected to show similar behaviour. This scheme also offers a useful first approximation to the interaction of swimmers with each other, which may be investigated more accurately using other techniques such as the reciprocal theorem [40]. The two-dimensional construction, while not appropriate to describe the most general cases of hydrodynamic interactions in the bulk of a three-dimensional fluid, nevertheless provides qualitative insight into behaviour of, for example, sedimented [13], floating [19] or confined [4] active matter.

A benefit of point-singularity models is that their simplicity means it should be possible to add additional swimmers external to the post, and study the resulting collective behaviour. We leave this for future work.

Acknowledgments

We thank Darren Crowdy and Marco Polin for useful discussions. This work was partially supported by EPSRC grant EP/E501311.

[1] M. C. Marchetti, J. F. Joanny, S. Ramaswamy, T. B. Liverpool, J. Prost, M. Rao, and R. A. Simha, Rev. Mod. Phys. **85**, 1143 (2013).
[2] R. Golestanian, T. B. Liverpool, and A. Adjari, Phys. Rev. Lett. **94** (2005).
[3] S. Ebbens, M. H. Tu, J. R. Howse, and R. Golestanian, Phys. Rev. E **85** (2012).
[4] I. Buttinoni, J. Bialké, F. Kümmel, H. Löwen, C. Bechinger, and T. Speck, Phys. Rev. Lett. **110** (2013).
[5] T. J. Pedley and J. O. Kessler, Annu. Rev. Fluid Mech. **24**, 313 (1992).
[6] E. Lauga and T. R. Powers, Rep. Prog. Phys. **72**, 096601 (2009).
[7] E. Lauga, W. R. DiLuzio, G. M. Whitesides, and H. A. Stone, Biophys. J. **90**, 400 (2006).
[8] A. P. Berke, L. Turner, H. C. Berg, and E. Lauga, Phys. Rev. Lett. **101**, 038102 (2008).
[9] K. Drescher, J. Dunkel, L. H. Cisneros, S. Ganguly, and R. E. Goldstein, Proc. Natl. Acad. Sci. U.S.A. **108**, 10940 (2011).
[10] V. Kantsler, J. Dunkel, M. Polin, and R. E. Goldstein, Proc. Natl. Acad. Sci. U.S.A. **110**, 1187 (2013).
[11] D. Lopez and E. Lauga, arXiv preprint arXiv:1406.4412 (2014).
[12] P. Denissenko, V. Kantsler, D. J. Smith, and J. Kirkman-Brown, Proc. Natl. Acad. Sci. U.S.A. **109**, 8007 (2012).
[13] D. Takagi, J. Palacci, A. B. Braunschweig, M. J. Shelley, and J. Zhang, Soft Matter **10**, 1784 (2014).
[14] K. Drescher, K. C. Leptos, I. Tuval, T. Ishikawa, T. J. Pedley, and R. E. Goldstein, Phys. Rev. Lett. **102**, 168101 (2009).
[15] K. C. Leptos, K. Y. Wan, M. Polin, I. Tuval, A. I. Pesci, and R. E. Goldstein, Phys. Rev. Lett. **111**, 158101 (2013).
[16] R. A. Simha and S. Ramaswamy, Phys. Rev. Lett. **89**, 058101_1 (2002).
[17] R. Voituriez, J. F. Joanny, and J. Prost, Europhys. Lett. **70**, 404 (2005).
[18] S. Ramaswamy, Annu. Rev. Condens. Matter Phys. **1**, 323 (2010).
[19] Y. Or and R. M. Murray, Phys. Rev. E **79**, 045302 (2009).
[20] D. G. Crowdy and Y. Or, Phys. Rev. E **81**, 036313 (2010).
[21] X.-L. Wu and A. Libchaber, Phys. Rev. Lett. **84**, 3017 (2000).
[22] N. Koumakis, A. Lepore, C. Maggi, and R. Di Leonardo, Nat. Commun. **4**, 2588 (2013).
[23] R. Di Leonardo, L. Angelani, D. Dell'Arciprete, G. Ruocco, V. Iebba, S. Schippa, M. P. Conte, F. Mecarini, F. De Angelis, and E. Di Fabrizio, Proc. Natl. Acad. Sci. U.S.A. **107**, 9541 (2010).
[24] K. Drescher, R. E. Goldstein, N. Michel, M. Polin, and I. Tuval, Phys. Rev. Lett. **105**, 168101 (2010).
[25] G. I. Taylor, Proc. R. Soc. Lond. A **209**, 447 (1951).
[26] T. Ishikawa, M. P. Simmonds, and T. J. Pedley, J. Fluid Mech. **568**, 119 (2006).
[27] G. P. Alexander and J. M. Yeomans, Europhys. Lett. **83**, 34006 (2008).
[28] E. Lauga and D. Bartolo, Phys. Rev. E **78**, 030901 (2008).
[29] M. J. Lighthill, Commun. Pure Appl. Math. **5**, 109 (1952).
[30] J. R. Blake, J. Fluid Mech. **46**, 199 (1971).
[31] G. P. Alexander, C. M. Pooley, and J. M. Yeomans, Phys. Rev. E **78**, 045302 (2008).
[32] D. J. Jeffrey and Y. Onishi, Q. J. Mech. Appl. Math. **34**, 129 (1981).
[33] S. Tanveer and G. L. Vasconcelos, J. Fluid Mech. **301**, 325 (1995).
[34] M. Siegel, SIAM J. Appl. Math. **59**, 1998 (1999).
[35] T. M. Squires and M. Z. Bazant, J. Fluid Mech. **509**, 217 (2004).
[36] D. G. Crowdy, J. Fluid Mech. **719**, R2 (2013).

[37] D. G. Crowdy, J. Fluid Mech. **735**, 473 (2013).
[38] W. E. Langlois, *Slow viscous flow* (Macmillan, 1964).
[39] J. R. Blake and A. T. Chwang, J. Eng. Math. **8**, 23 (1974).
[40] D. Papavassiliou and G. P. Alexander (2014), in preparation.